ACS APPLIED MATERIALS & INTERFACES

Research Article

www.acsami.org

Small-Scale, Self-Propagating Combustion Realized with On-Chip Porous Silicon

Nicholas W. Piekiel* and Christopher J. Morris

U.S. Army Research Laboratory, Adelphi, Maryland 20783, United States

Supporting Information

ABSTRACT: For small-scale energy applications, energetic materials represent a high energy density source that, in certain cases, can be accessed with a very small amount of energy input. Recent advances in microprocessing techniques allow for the implementation of a porous silicon energetic material onto a crystalline silicon wafer at the microscale; however, combustion at a small length scale remains to be fully investigated, particularly with regards to the limitations of increased relative heat loss during combustion. The present study explores the critical dimensions of an on-chip porous silicon energetic material (porous silicon + sodium perchlorate ($NaClO_4$)) required to propagate combustion. We etched ~97 μm wide and ~45 μm deep porous silicon channels that burned at a steady rate of 4.6 m/s, remaining steady across 90° changes in direction. In an effort to minimize the potential on-chip footprint for energetic porous silicon, we also explored the minimum spacing between porous silicon channels. We demonstrated independent burning of porous silicon channels at a spacing of <40 μm. Using this spacing, it was possible to have a flame path length of >0.5 m on a chip surface area of 1.65 cm^2. Smaller porous silicon channels of ~28 μm wide and ~14 μm deep were also utilized. These samples propagated combustion, but at times, did so unsteadily. This result may suggest that we are approaching a critical length scale for self-propagating combustion in a porous silicon energetic material.

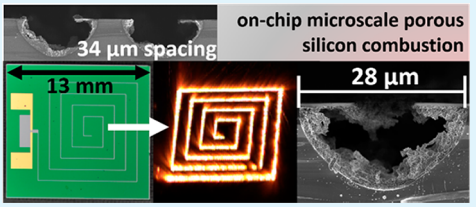

KEYWORDS: *microscale combustion, porous silicon, on-chip, energetic materials*

1. INTRODUCTION

An on-chip energetic material is a high energy density system implemented onto or within a microscale device. This ideally provides a large potential energy that can be accessed by initiation with the small amounts of energy available in microelectromechanical systems (MEMS). There are many potential applications for on-chip energetic materials including micropropulsion,[1−5] initiation of other energetic materials,[6−8] or reactive bonding[9,10] because materials can be selected or tuned to optimize gas, heat, or light production. A handful of materials including porous silicon, nanothermites, reactive foils, and traditional high explosives have been utilized in conjunction with microscale systems. However, the energetic material itself is often implemented at the millimeter scale or greater. Ideally, for implementation and use in microscale devices, the energetic materials should also have a characteristic size on the same submillimeter scale. Scaling energetic materials requires addressing several practical issues, namely the fine patterning of energetics and heat losses during combustion at the microscale.[11]

For energetic material combustion propagation, heat from the reaction must efficiently dissipate to a neighboring region of unreacted energetic material for it to reach its ignition temperature and continue the reaction. When dealing with confined or embedded energetic materials, heat transfer properties of the surrounding materials are often superior to those of the energetic material itself, which can result in considerable heat loss. For small-scale energetic materials, where total energy production is considerably less than that of a bulk energetic material, heat loss to surrounding materials can be enough to quench the reaction. There are limited studies investigating combustion propagation for energetic materials where the characteristic length scale is below 1 mm. In one such study, Tappan et al. demonstrate propagation of lead styphnate at <100 m/s in confined silicon-based microchannels 300 μm wide and 100 μm deep.[12] In a study using similarly sized stainless steel microchannels, an Al/MoO_3 thermite composite shows combustion propagation at a minimum cross section of 299 μm wide and 76.2 μm deep and a hydraulic diameter of 121 μm.[13] Propagation at the smallest channel dimension of this study is observed to be unsteady, but the authors suggest that propagation is possible down to even smaller length scales.

Several recent advances in patterning and printing technologies allow for microscale application of energetic materials onto a substrate or electrode. These methods include deposition,[12,14−20] spin-coating,[21−23] or direct writing.[21,24] Deposition demonstrates considerable promise due to the simplicity of the process and vast material compatibility. Notable studies include the microscale patterning of pentaerythritol tetranitrate (PETN) through deposition on a silicon surface using physical vapor deposition (PVD) and a silicon oxide "lift-off" layer.[12,18] A similar vapor deposition technique is possible for hexanitroazobenzene (HNAB) deposition,[14]

Received: March 4, 2015
Accepted: April 21, 2015
Published: April 21, 2015

DOI: 10.1021/acsami.5b01964
ACS Appl. Mater. Interfaces 2015, 7, 9889−9897

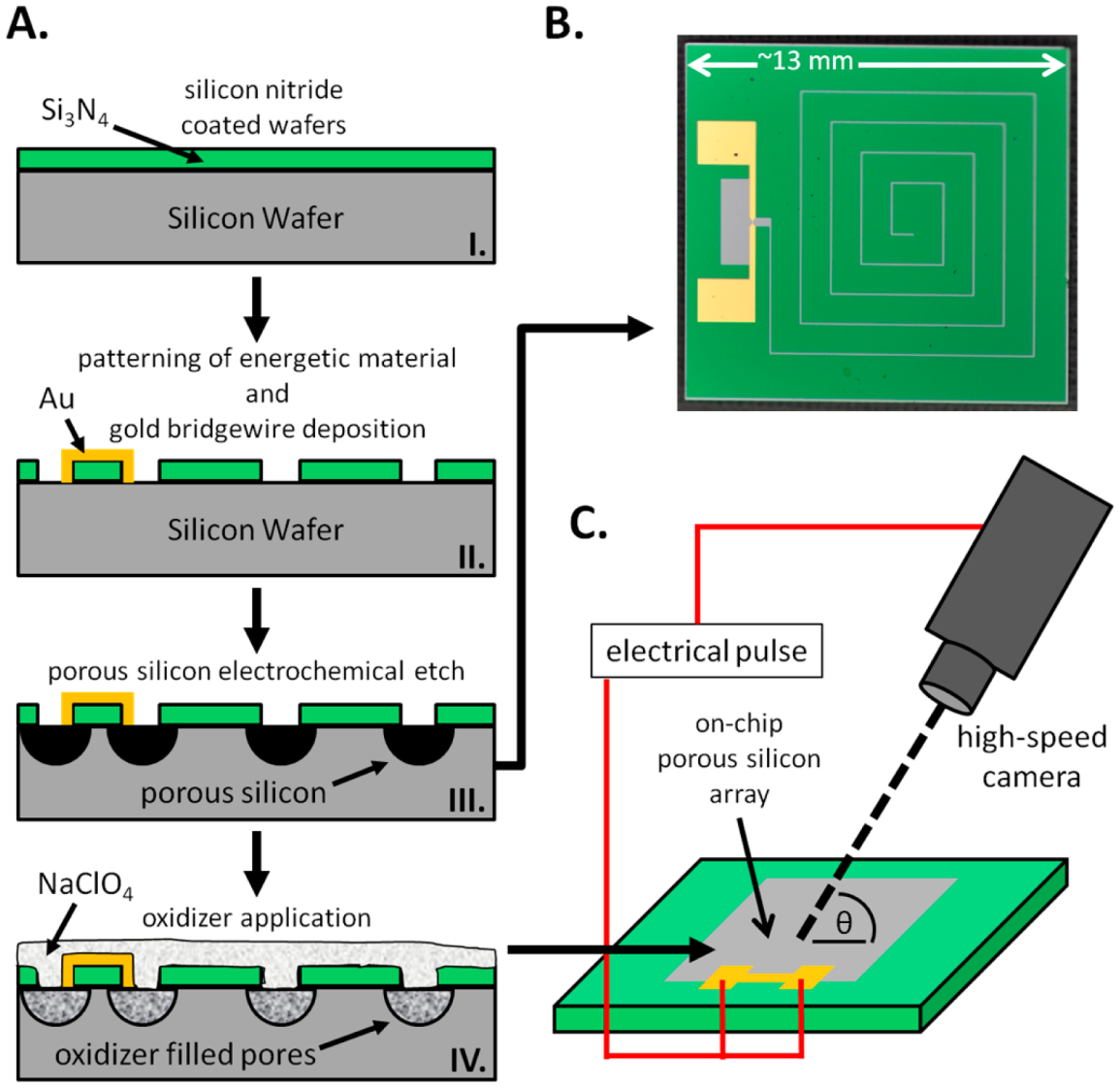

Figure 1. (A) Fabrication steps for the porous silicon energetic material formation. (I) Initial wafer with Si_3N_4 protective layer (the backside platinum electrode is not pictured). (II) Photolithography used to selectively remove Si_3N_4 and the gold bridge wire was applied through sputter deposition. (III) Galvanic etch used to form porous silicon. (IV) Oxidizer applied to the sample. (B) Picture of a sample with a winding porous silicon channel. (C) Schematic of the experimental setup for imaging of the winding porous silicon channels. The camera was placed at a slight angle (θ) requiring a distance conversion when tracking flame travel (Supporting Information).

suggesting that this method may be suitable for a number of explosive energetic materials. Nanothermites are patterned in a similar method using the inherent charge of the metal and metal oxide nanoparticles in solution to electrophoretically deposit a film onto a charged electrode.[15,16] In a tapered width test experiment, unconfined Al/CuO films of ~10 μm thickness and a width variation of 400−10 μm demonstrate complete combustion.[16] Smaller scale production of energetic materials is possible, as spin-coating techniques produce features on the order of 1−10 μm,[21,23] and inkjet printing produces samples as small as ~90 ng for trace explosive detection studies.[24] In these particular studies at the microscale, combustion behavior is not explored; however, an actuation study utilizing a cobalt−manganese-based energetic material demonstrates combustion for samples down to ~90 ng.[25] Although this study demonstrates combustion for a very small sample size, the self-propagation of confined or embedded samples at such small scales remains to be explored. Reactive nanolaminates are another class of energetic material that commonly demonstrate combustion propagation for film thicknesses on the order of 10 μm, but they are typically only constrained in one dimension (thickness).[26,27] In one case where two dimensions were constrained for reactive bonding purposes, nanolaminates made of aluminum and palladium with a total thickness of <2.5 μm demonstrated steady propagation down to a lateral width of 20 μm.[28]

Another unique method for microscale energetic material implementation is through porous silicon etching. When combined with an appropriate oxidizer, porous silicon is an attractive energetic material and has recently garnered significant research attention.[29−38] Patterning of porous silicon features is performed with relative ease using standard photolithography techniques and a protective masking layer on the wafer surface such as silicon nitride (Si_3N_4)[29,33−36,39−42] or photoresist.[42] The combustion process is the subject of several comprehensive studies,[35,38] demonstrating a wide range

DOI: 10.1021/acsami.5b01964
ACS Appl. Mater. Interfaces 2015, 7, 9889−9897

of combustion performance with unconfined flame speeds in the range of 1[31,38] to 3600 m/s[36] for on-chip systems. Although the planar feature size of samples for porous silicon combustion studies is typically several millimeters or more, the utilized microfabrication techniques are capable of producing features on the microscale with relative ease. In the present study, we employ a galvanic porous silicon etch technique[29,35,43,44] to implement microscale porous silicon channels on-chip. This method allowed for variation of the porous silicon pattern, which permitted implementation of several experiments onto a single sample. For porous silicon channels that were ∼97 μm wide, we investigated the propagation speed and the minimum spacing between channels that allowed for independent propagation. We also examined combustion propagation in smaller channels of 28 × 14 μm. These channels were among the smallest to demonstrate on-chip combustion propagation, to date.

2. EXPERIMENTAL SECTION

2.1. Formation of Porous Silicon Energetic Material. Galvanically etched porous silicon was formed on <0.01 Ω·cm resistivity, ⟨100⟩ orientation, boron doped, *p*-type silicon wafers with a double-sided silicon nitride (Si_3N_4) layer from Rogue Valley Microdevices (Medford, OR). The primary steps of the on-chip energetic material fabrication process are depicted in Figure 1A, and detailed explanations of the galvanic etch process are detailed elsewhere.[29,43,44] In short, the galvanic porous silicon etch utilizes the inherent charge carriers of the silicon wafer and a platinum coating on the wafer backside to electrochemically etch the silicon when placed in a solution of hydrofluoric acid (HF), ethanol (EtOH), and hydrogen peroxide (H_2O_2). For platinum deposition, the backside Si_3N_4 was removed to allow for a sputter process by LGA Thin Films, Inc. (Santa Clara, CA, USA). The frontside Si_3N_4 layer was selectively removed through a photolithography process to create the desired pattern for porous silicon. A resulting sample after the photolithography process is shown in Figure 1B. Various patterns of porous silicon were used with the "pre-etch" channel width designed to be either 10 or 50 μm. Although these widths were precisely designed in the photolithography process, an undercutting effect[29,45] of the etch process increased the actual channel width, which we determined with scanning electron microscopy (SEM). After selective removal of Si_3N_4, the wafer was diced into individual strips that were placed into the etching solution for a set amount of time depending on the desired etch depth. The makeup of the etch solution has a significant effect on the final porous silicon film, and in this case, the solution was a 3:1 volumetric ratio of HF/EtOH with 2.4% H_2O_2 added afterward. Following porous silicon formation, sodium perchlorate ($NaClO_4$) was drop cast in a nearly saturated 3.2 M solution onto the wafer surface. The solution then seeped into the pores of the porous silicon to form the energetic composite and was dried for ∼30 min in a nitrogen environment.

2.2. High-Speed Video Analysis. After the energetic material dried, an electrical pulse triggered the energetic reaction through joule heating of a patterned gold bridgewire.[29,39] This same electrical pulse simultaneously began an image capture process with a Photron FASTCAM SA5 high-speed camera at 60 000 frames per second (fps). A schematic of the experimental setup is provided in Figure 1C. This figure shows that the camera placement was at a slight angle due to space restrictions above the porous silicon samples. Due to this camera angle, we performed additional calculations to determine the flame travel distance; these calculations are included in the Supporting Information. All combustion tests were performed in a nitrogen environment due to the hygroscopic nature of $NaClO_4$, and were unconfined.

Flame speed analysis was performed using the individual images taken with the high speed camera. To visually represent the flame path through the porous silicon channels, MATLAB was used to create a single agglomerate image of up to several thousand consecutive images. These images were taken during the combustion process and represent the overall flame path. The MATLAB program was used to evaluate the individual high-speed images sequentially, where for each image, the red, green, and blue (RGB) values were summed for each pixel and were compared with the RGB sum of the identical pixel of the previous image. When the pixels from one image were compared to the next, the higher color value for each of the red, green, or blue values was retained. This effectively kept the brightest pixels of the two images for comparison with the next image. The result was that only the bright features of all images were represented in one final image. This image alteration process began a set number of images after the ignition process, as ignition led to a larger flame that optically saturated part of the remaining flame path.

A similar method was used to plot the flame movement through the chip and to determine the total distance traveled as a function of time. For each image, the location of the brightest pixel was taken as the flame location. For this analysis a 25% threshold intensity was used to avoid potential noise from bright areas outside of the flame path. The location was recorded and plotted for each image to track flame movement. These data were also fit with a Savitzky−Golay filter[46] to better represent the traveled distance.

3. RESULTS AND DISCUSSION

3.1. Demonstration of Small-Scale Porous Silicon Combustion and Flame Tracking. The small-scale channels were patterned on-chip in a spiral pattern to investigate the ability of the energetic material to change direction and propagate steadily. The width of the as-designed 50 μm wide channels was actually 97 μm due to undercutting of the etch, as shown in Figure 2A.

Although Figure 2A was acquired following a combustion event, the cross-sectional dimensions of the PS channel were the same before combustion. An agglomerate image of 1080 high-speed images of the flame propagation is shown in Figure 3A. The image collecting process for Figure 3A began at ∼1.2 ms to avoid saturation from the flame after the ignition process. The inlay of Figure 3A is a single video frame (cropped, but at the same scale) from this combustion event. The tracking of the combustion front is shown in Figure 3B, depicting a continual flame front without the presence of jumping between parallel channels of the porous silicon. We note that in Figure 3A, in the bottom right part of the image, a dark region exists in the flame path. This region appears to be a section of the channel with inconsistent burning, which may have been due to inadequate oxidizer application in that region. The distance traveled by the flame as a function of time is plotted in Figure 3C demonstrating a total length of ∼85 mm at an average velocity of 4.6 m/s. The actual traveled distance for the flame was ∼87 mm, suggesting there was some error in the flame distance calculation; however, this error was relatively small at 2%. From the plot in Figure 3C it is observed that the flame propagation was steady throughout the combustion process despite the 90° bends negotiated along the propagation path.

3.2. Determination of Minimum Spacing for Porous Silicon Combustion. To investigate the minimum allowed spacing for independent burning of porous silicon channels, we implemented a single winding porous silicon channel with decreasing channel spacing, as shown in Figure 4A. On this sample there were eight different spacings for the porous silicon channel, which are labeled individually in Figure 4A. The designed spacing values (ranging from 5 to 3500 μm) are provided in Table 1. Due to the undercutting effect of the porous silicon etch, the actual spacings were smaller than designed. The actual spacing distance was measured using SEM for sections 5, 6, and 7, and the spacing was consistently 66 μm

DOI: 10.1021/acsami.5b01964
ACS Appl. Mater. Interfaces 2015, 7, 9889−9897

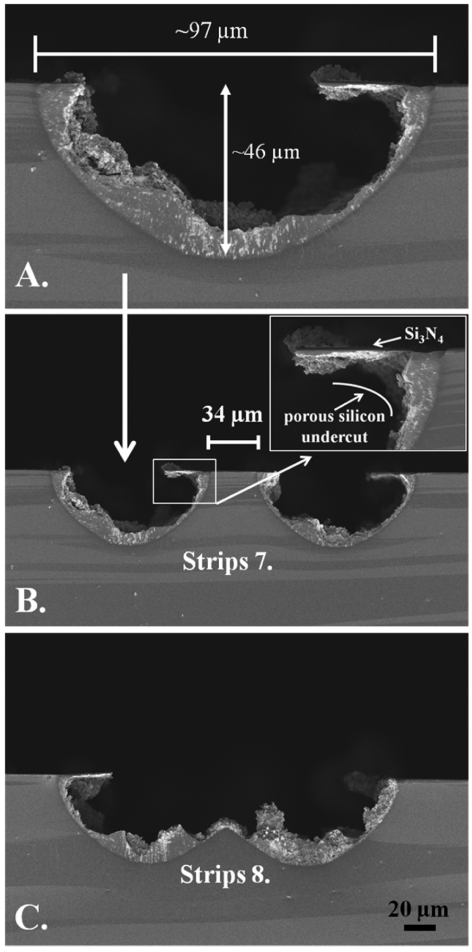

Figure 2. (A) Postcombustion SEM image of the cross-section of the sample in Figure 4. Identical etch conditions were used for the sample in Figure 3. (B) SEM cross-section image of sections 7 from Figure 4. (C) SEM cross-section image of section 8 from Figure 4. We note the spacing in section 7 and 8 was much smaller than originally designed due to undercutting during the porous silicon etch.

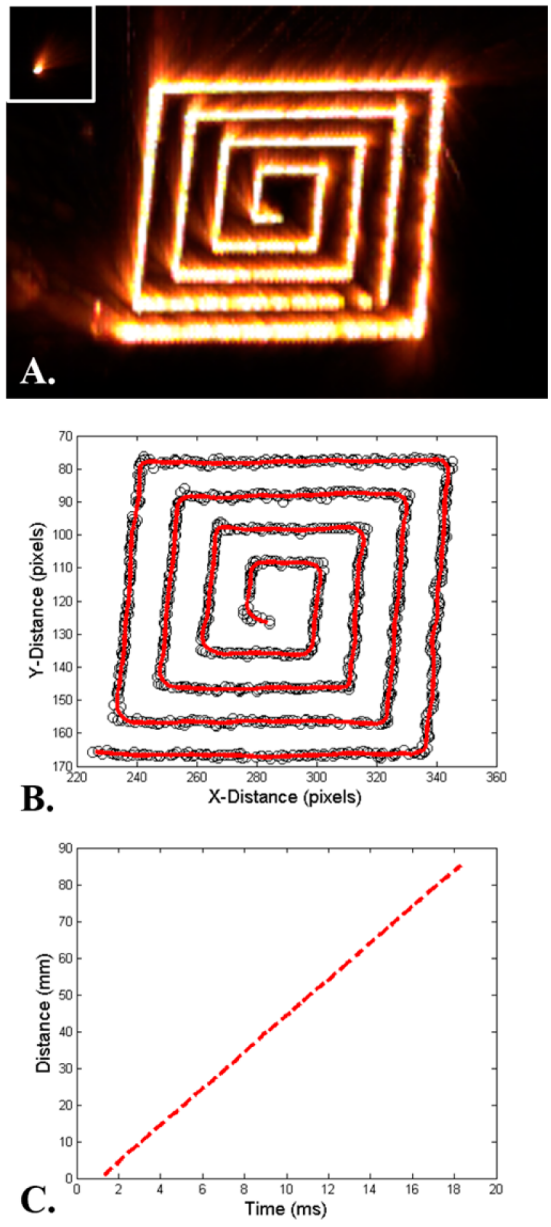

Figure 3. (A) Agglomerate image of a combusting porous silicon spiral channel with a width of 97 μm, compiled from 1080 images taken at 60 000 fps. (B) Tracked flame position throughout the combustion process in panel A. (C) Distance traveled by the flame with respect to time.

smaller than designed. This value was used to calculate actual spacing for the sections with larger spacing distances in Table 1.

From the flame tracking in Figure 4B it is apparent that all of the porous silicon sections were involved in the reaction, even at the smallest spacing, however it is not clear that the channels with the smallest spacing burned independently. An expanded plot of the closely packed porous silicon channels is provided in Figure 4C. For the sections of porous silicon 1−7, it is evident that each porous silicon channel burned independently in Figure 4B and Figure 4C, but set 8 burned as one channel, as is evident in Figure 4C. Inspection via SEM of section 7 and 8 in Figure 2B and Figure 2C shows the 34 μm spacing for section 7, but also shows that the undercutting etch resulted in a single porous silicon strip for section 8. This explains the burning behavior for section 8 as a single strip, but also demonstrates that independent burning of porous silicon strips is possible at a spacing of ~34 μm. In separate experiments, a spacing of ~4 μm was utilized, but failed to yield independent burning.

To further demonstrate the ability of closely packed porous silicon channels to propagate independently, we implemented an array of winding porous silicon channels with spacing similar to that of Figure 2A at 34 μm. Figure 5A shows a sample with closely packed, winding porous silicon channels. It was expected that this sample would burn independently throughout the entire chip; however, as shown in Figure 5B, we observed some inconsistencies in the burning path. Below the plot in Figure 5B, images are included to demonstrate the burning in each region. For each of the sections showing inconsistencies (Figure 5B I, II, and IV), we observed multiple sections burning at once. Despite these few sections with inconsistent burning, the majority of the chip burned as designed with the channels burning independently as in Figure 5B III. With the winding structure tested in this study, the total flame path length was ~0.51 m, which with a propagation speed of 4.6 m/s could produce a burn time of up to 111 ms.

3.3. Heat Transfer for Closely Packed Porous Silicon Channels. The simultaneous combustion propagation for the closely packed channels in Figure 5B I, II, and IV could be

DOI: 10.1021/acsami.5b01964
ACS Appl. Mater. Interfaces 2015, 7, 9889−9897

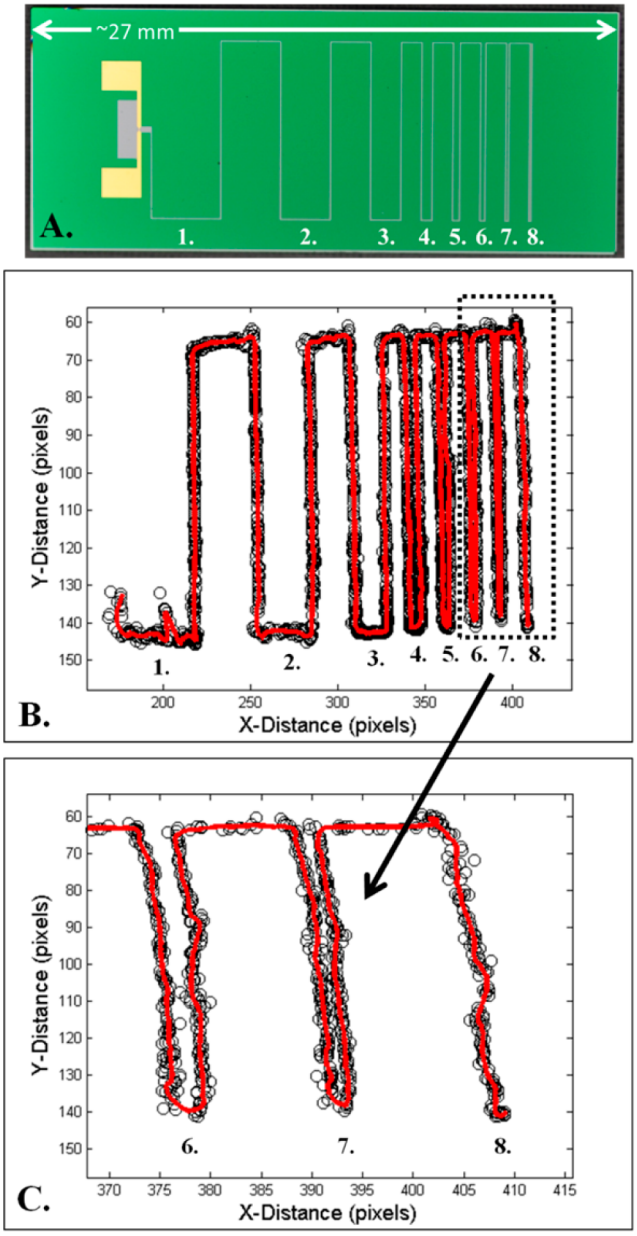

Figure 4. (A) Picture of the winding porous silicon channels designed for testing the critical channel spacing for independent burning. (B) The tracked flame position throughout the combustion process for the sample in panel A. (C) Magnified view of the tracked flame position for sections 6−8 of the spaced porous silicon channels.

Table 1. Designed and Measured Spacing Distance for Each Section of the Porous Silicon Channel in Figure 4

porous silicon channel group	designed spacing (μm)	actual spacing (μm)
1	3500	3434
2	2500	2434
3	1500	1434
4	500	434
5	300	234
6	200	134
7	100	34
8	50	0

caused by advection of hot particles across the short spacing between the channels, or by heat conduction through the substrate. Hot particle advection has demonstrated ignition of samples at large spacing compared to the length scales of this study.[16] Although particle advection could be a concern for the combustion of these closely packed porous silicon channels, the independent burning of the majority of the sample in Figure 5B leads us to believe that the embedded state of the channels helped to prevent ignition from particle advection.

To investigate the role of heat conduction at this small spacing, we calculated the temperature change through the closely packed silicon channels using eq 1 for transient heat conduction through a semi-infinite slab with a constant-temperature boundary condition at the surface:[47]

$$T_u(x, t) = (T_i - T_s)\,\mathrm{erf}\left(\frac{x}{2\sqrt{\alpha t}}\right) + T_s \quad (1)$$

where, T_s is the surface temperature at the junction between porous silicon and crystalline silicon during combustion, T_i is the ambient temperature, T_u is the temperature at the unreacted surface in Figure 6B, and α is the thermal diffusivity of silicon at room temperature (9.1×10^{-5} m^2 s^{-1}).

The resulting temperature calculations are shown in Figure 6A, assuming a constant temperature for T_s at the melting point of silicon, 1687 K. After 5 μs, the temperature at the unreacted porous silicon surface (T_u) is at 660 K, already over the ignition temperature of the PS/$NaClO_4$ system under slow heating conditions (~537 K).[48] Considering the reaction speed for the 97 μm channels is ~4.6 m/s, an assumed 100 μm wide reaction zone would hold T_s at this constant surface temperature for a characteristic time of 22 μs; more than the 5 μs required to heat an adjacent channel to its ignition temperature.

Based on this heat conduction calculation with a temperature boundary condition of 1687 K, few, if any, of the channels in Figure 5 ought to burn independently. The fact that we observed most of them burn independently suggests that we have overpredicted T_s and/or oversimplified the model. One factor that may result in a reduced temperature at T_s is the residue observed at T_s in Figure 2. Energy dispersive X-ray spectroscopy (EDX) was performed on this residue during SEM. The results show that the primary element in this residue is silicon, although the surrounding crystalline silicon could have skewed this result. As expected, other elements present were Na, Cl, and O. At this time we cannot definitively conclude the makeup of this residue, but we believe it was a combination of unreacted porous silicon, and the reaction products NaCl and SiO_2. Assuming the residue is primarily unreacted porous silicon, the lower thermal conductivity of the residue would result in a temperature drop between the actual reaction temperature and the boundary temperature T_s used in the model. A lower T_s value would allow most or all of the channels to burn independently, which seems plausible given the experimental results observed. Additional analysis is necessary to better quantify this effect, but the basic heat transfer analysis presented here is useful to show how one may go about designing closely packed adjacent energetic channels. The analysis also shows that we may be near the spacing limit for these porous silicon channels.

3.4. Combustion Propagation at Smaller Scales. With the 97 μm wide porous silicon channels, we observed steady burning. To investigate even smaller channels, we implemented a designed 10 μm wide winding channel with a similar spacing setup as that in Figure 4A. After the undercutting of the Si_3N_4, the actual porous silicon channel was much wider at 28 μm

DOI: 10.1021/acsami.5b01964
ACS Appl. Mater. Interfaces 2015, 7, 9889−9897

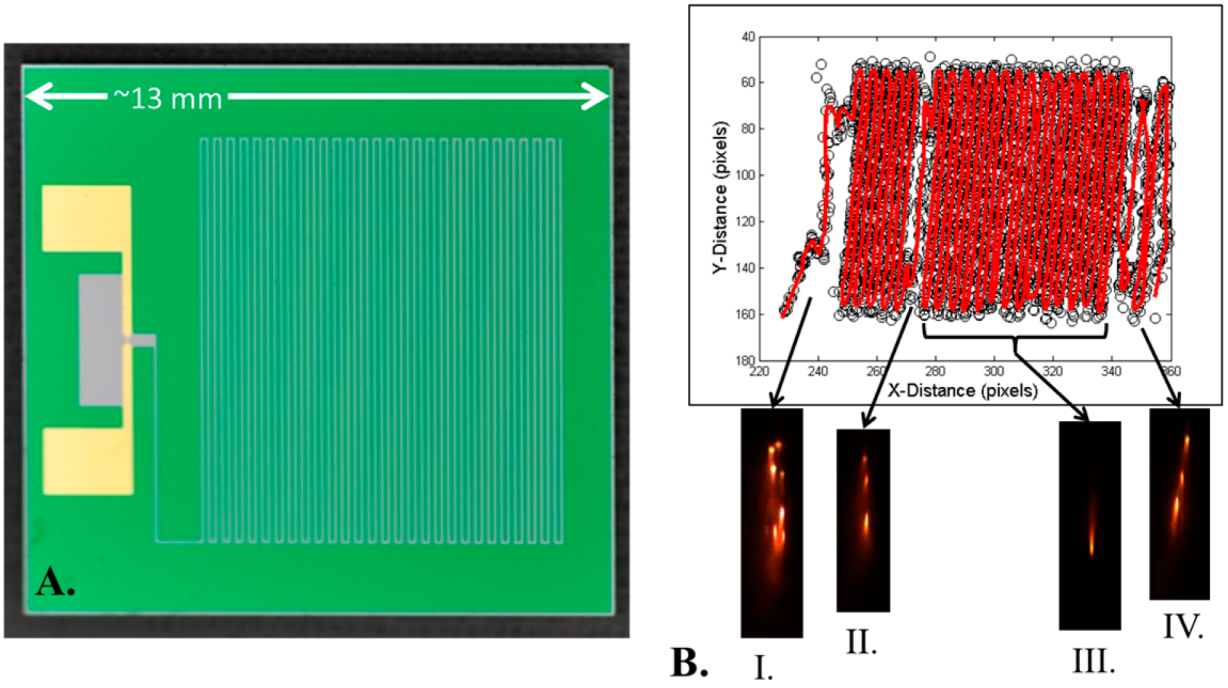

Figure 5. (A) Winding porous silicon channel designed with 97 μm spacing and an actual spacing similar to that in Figure 2A. (B) The tracked flame position throughout the combustion process in panel A. The embedded images are single images taken from the indicated positions during the flame travel to identify the burning behavior in each section.

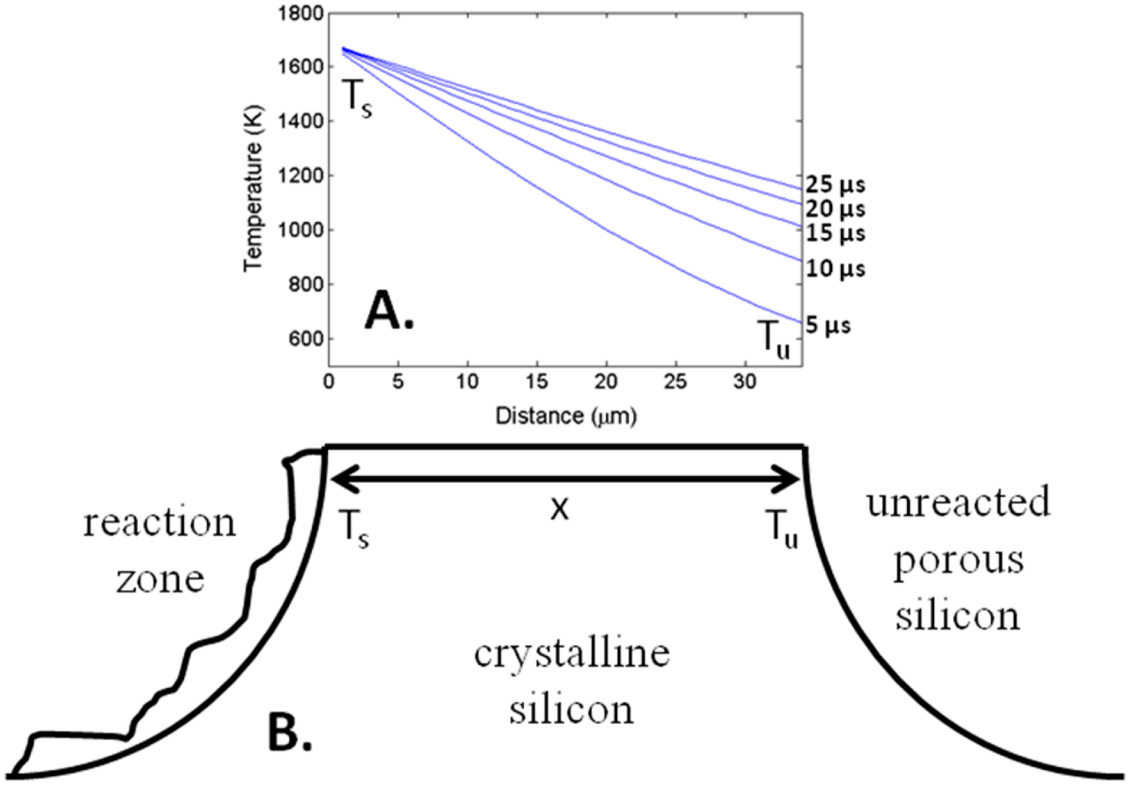

Figure 6. (A) Transient heat conduction model through crystalline silicon at 5 μs intervals for the model shown in Figure 6B. (B) Schematic for heat transfer calculation during combustion for the closely packed ~100 μm porous silicon channels from Figure 5

with a nearly semicircular cross section with a radius of 14 μm, as shown in Figure 7.

Flame tracking during combustion for this sample is shown in Figure 7B, and the distance tracking is presented in Figure 7C. At the start of combustion in Figure 7 panels B and C, it is clear that there was unsteady combustion propagation. This unsteadiness may indicate the nearing of a critical dimension for combustion propagation but could also be due to uneven oxidizer application in this region. The current method of oxidizer application leaves considerable residue on the surface,

DOI: 10.1021/acsami.5b01964
ACS Appl. Mater. Interfaces 2015, 7, 9889−9897

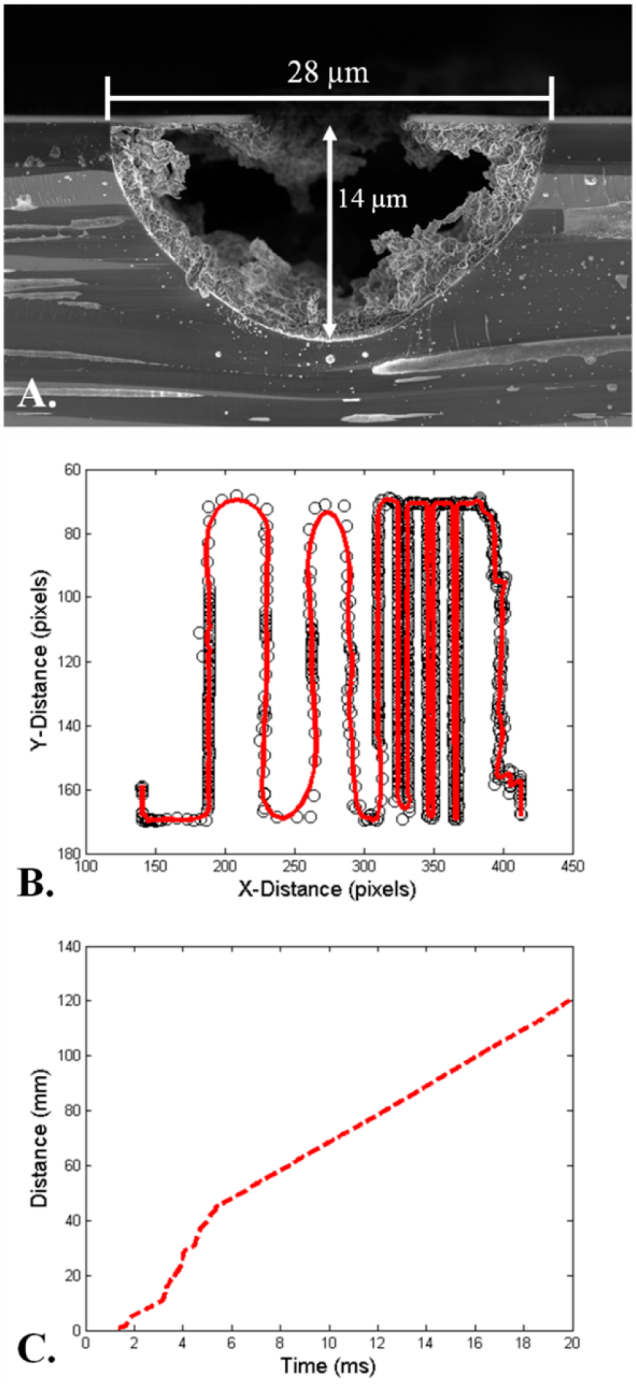

Figure 7. (A) SEM image of a small porous silicon channel measuring ~28 × 14 μm. (B) Flame tracking for combustion propagation for the sample from panel A, which had a similar flame path as that in Figure 4A. (C) Distance tracking for combustion propagation for the sample in panel A.

and this potential source of variability should be addressed in future studies. In Figure 7C, at $t > 5$ ms, the flame propagation becomes steady at 5.2 m/s, very close to the 4.6 m/s flame speed demonstrated for the propagation in Figure 3. It is important to note that despite a region of unsteady propagation at the start of combustion, the steady propagation for the rest of the sample shows that steady propagation is possible for channels at this length scale. Although this combustion occurred in a much smaller channel, the flame speed is on the same order as the flame speed through similar material at a larger scale. We previously investigated combustion through 54 μm deep, 3 mm wide strips of porous silicon using an identical etch solution and demonstrated a flame speed of 8.0 ± 0.6 m/s.[35]

4. CONCLUSIONS

This study demonstrated combustion processes for small-scale porous silicon channels patterned on-chip. The results were among the smallest steady combustion propagation events reported to-date, as we observed a 4.6 m/s propagation speed in porous silicon channels with cross-sectional dimensions of 97 × 46 μm. For even smaller channels of ~28 × 14 μm, the combustion propagation started unsteadily but eventually transitioned to a steady combustion at 5.2 m/s. The unsteady combustion may have been due to heat losses to the surrounding substrate but could also be due to uneven oxidizer application. Aside from small-scale combustion, we patterned individual channels in close proximity to investigate the spacing limit. At a spacing of <40 μm, independent burning of 97 μm wide porous silicon channels was still observed. This provides the capability to introduce long flame paths, on the order of 1 m, on a ~1 cm^2 chip surface area. For applications requiring delays, or longer burn times, this capability could be an attractive option. First order heat transfer calculations suggest that for porous silicon combustion we are nearing the length scale limits for minimum spacing. While some inconsistencies are still apparent, this technology shows the ability to drastically reduce the on-chip footprint for energetic materials use with MEMS while still demonstrating the ability to achieve steady combustion events. Further studies are required to confirm the limits of combustion for porous silicon at these length scales, and ideally, novel ways to reduce this scale to even smaller lengths may be realized.

■ ASSOCIATED CONTENT

Ⓢ Supporting Information

Additional information on the flame speed calculations and compensation for camera angle indicated in Figure 1C. The Supporting Information is available free of charge on the ACS Publications website at DOI: 10.1021/acsami.5b01964.

■ AUTHOR INFORMATION

Corresponding Author

*E-mail: nicholas.piekiel.civ@mail.mil.

Notes

The authors declare no competing financial interest.

■ ACKNOWLEDGMENTS

The authors would like to acknowledge Brian Isaacson for assistance in sample fabrication.

■ REFERENCES

(1) Churaman, W.; Currano, L.; Morris, C.; Rajkowski, J.; Bergbreiter, S. The First Launch of an Autonomous Thrust-Driven Microrobot Using Nanoporous Energetic Silicon. *J. Microelectromech. Syst.* **2012**, *21* (1), 198−205.

(2) Churaman, W.; Morris, C.; Currano, L.; Bergbreiter, S. On-Chip Porous Silicon Microthruster for Robotic Platforms*Transducers Eurosensors XXVII: The 17th International Conference on Solid-State Sensors, Actuators, and Microsystems, 2013*, Barcelona, Spain, June 16−20, 2013; pp 1599−1602.

DOI: 10.1021/acsami.5b01964
ACS Appl. Mater. Interfaces 2015, 7, 9889−9897

(3) Staley, C. S.; Raymond, K. E.; Thiruvengadathan, R.; Apperson, S. J.; Gangopadhyay, K.; Swaszek, S. M.; Taylor, R. J.; Gangopadhyay, S. Fast-Impulse Nanothermite Solid-Propellant Miniaturized Thrusters. *J. Propul. Power* **2013**, *29* (6), 1400−1409.
(4) Zhang, K.; Chou, S.; Ang, S.; Tang, X. A MEMS-Based Solid Propellant Microthruster with Au/Ti Igniter. *Sens. Actuators, A* **2005**, *122* (1), 113−123.
(5) Zhang, K. L.; Chou, S. K.; Ang, S. S. Development of a Solid Propellant Microthruster with Chamber and Nozzle Etched on a Wafer Surface. *J. Micromech. Microeng.* **2004**, *14* (6), 785.
(6) Guo, R.; Hu, Y.; Shen, R.; Ye, Y.; Wu, L. A Micro Initiator Realized by Integrating KNO_3@CNTs Nanoenergetic Materials with a Cu Microbridge. *Chem. Eng. J. (Amsterdam, Neth.)* **2012**, *211−212* (0), 31−36.
(7) Staley, C. S.; Morris, C. J.; Thiruvengadathan, R.; Apperson, S. J.; Gangopadhyay, K.; Gangopadhyay, S. Silicon-Based Bridge Wire Micro-Chip Initiators for Bismuth Oxide-Aluminum Nanothermite. *J. Micromech. Microeng.* **2011**, *21* (11), 115015.
(8) Taton, G.; Lagrange, D.; Conedera, V.; Renaud, L.; Rossi, C. Micro-Chip Initiator Realized by Integrating Al/CuO Multilayer Nanothermite on Polymeric Membrane. *J. Micromech. Microeng.* **2013**, *23* (10), 105009.
(9) Braeuer, J.; Besser, J.; Wiemer, M.; Gessner, T. A Novel Technique for MEMS Packaging: Reactive Bonding with Integrated Material Systems. *Sens. Actuators, A* **2012**, *188* (0), 212−219.
(10) Qiu, X.; Wang, J. Bonding Silicon Wafers with Reactive Multilayer Foils. *Sens. Actuators, A* **2008**, *141* (2), 476−481.
(11) Tappan, A. S. There's Plenty of Room in the Middle−Microenergetics, the Mesoscale, and Interfaces. *Propellants, Explos., Pyrotech.* **2013**, *38* (4), 475−475.
(12) Tappan, A. S.; Renlund, A. M.; Long, G. T.; Kravitz, S. H.; Erickson, K. L.; Trott, W. M.; Baer, M. R. Microenergetic Processing and Testing to Determine Energetic Material Properties at the Mesoscale. In *Proceedings of the 12th International Detonation Symposium*, San Diego, California, Aug 11−16, 2002; pp 3−10.
(13) Son, S. F.; Asay, B. W.; Foley, T. J.; Yetter, R. A.; Wu, M. H.; Risha, G. A. Combustion of Nanoscale Al/MoO_3 Thermite in Microchannels. *J. Propul. Power* **2007**, *23* (4), 715−721.
(14) Knepper, R.; Browning, K.; Wixom, R. R.; Tappan, A. S.; Rodriguez, M. A.; Alam, M. K. Microstructure Evolution during Crystallization of Vapor-Deposited Hexanitroazobenzene Films. *Propellants, Explos., Pyrotech.* **2012**, *37* (4), 459−467.
(15) Sullivan, K. T.; Kuntz, J. D.; Gash, A. E. Electrophoretic Deposition and Mechanistic Studies of Nano-Al/CuO Thermites. *J. Appl. Phys.* **2012**, *112* (2), 024316.
(16) Sullivan, K. T.; Kuntz, J. D.; Gash, A. E. Fine Patterning of Thermites for Mechanistic Studies and Microenergetic Applications. *Int. J. Energy Mater. Chem. Propul.* **2013**, *12* (6), 511−528.
(17) Tappan, A. S.; Knepper, R.; Wixom, R. R.; Marquez, M. P.; Ball, J. P.; Miller, J. C. Critical Detonation Thickness in Vapor-Deposited Pentaerythritol Tetranitrate (PETN) Films. *AIP Conf. Proc.* **2012**, *1426* (1), 677−680.
(18) Tappan, A. S.; Wixom, R. R.; Trott, W. M.; Long, G. T.; Knepper, R.; Brundage, A. L.; Jones, D. A. Microenergetic Shock Initiation Studies on Deposited Films of PETN. *AIP Conf. Proc.* **2009**, *1195* (1), 319−322.
(19) Zhang, K.; Rossi, C.; Ardila Rodriguez, G.; Tenailleau, C.; Alphonse, P. Development of a Nano-Al/CuO Based Energetic Material on Silicon Substrate. *Appl. Phys. Lett.* **2007**, *91* (11), 113117−113117−3.
(20) Zhang, K.; Rossi, C.; Petrantoni, M.; Mauran, N. A Nano Initiator Realized by Integrating Al/CuO-Based Nanoenergetic Materials With a Au/Pt/Cr Microheater. *J. Microelectromech. Syst.* **2008**, *17* (4), 832−836.
(21) Nafday, O.; Pitchimani, R.; Weeks, B.; Haaheim, J. Patterning High Explosives at the Nanoscale. *Propellants, Explos., Pyrotech.* **2006**, *31* (5), 376−381.
(22) Zhang, G.; Sun, H.; Abbott, J. M.; Weeks, B. L. Engineering the Microstructure of Organic Energetic Materials. *ACS Appl. Mater. Interfaces* **2009**, *1* (5), 1086−1089.
(23) Zhang, X.; Weeks, B. L. Tip Induced Crystallization Lithography. *J. Am. Chem. Soc.* **2014**, *136* (4), 1253−1255.
(24) Windsor, E.; Najarro, M.; Bloom, A.; Benner, B.; Fletcher, R.; Lareau, R.; Gillen, G. Application of Inkjet Printing Technology to Produce Test Materials of 1,3,5-Trinitro-1,3,5 Triazcyclohexane for Trace Explosive Analysis. *Anal. Chem.* **2010**, *82* (20), 8519−8524.
(25) Rodriguez, G. A. A.; Suhard, S.; Rossi, C.; EstÃve, D.; Fau, P.; Sabo-Etienne, S.; Mingotaud, A. F.; Mauzac, M.; Chaudret, B. A Microactuator Based on the Decomposition of an Energetic Material for Disposable Lab-on-Chip Applications: Fabrication and Test. *J. Micromech. Microeng.* **2009**, *19* (1), 015006.
(26) Gavens, A. J.; Van Heerden, D.; Mann, A. B.; Reiss, M. E.; Weihs, T. P. Effect of Intermixing on Self-Propagating Exothermic Reactions in Al/Ni Nanolaminate Foils. *J. Appl. Phys.* **2000**, *87* (3), 1255−1263.
(27) Adams, D. Reactive Multilayers Fabricated by Vapor Deposition: A Critical Review. *Thin Solid Films* **2015**, *576*, 98−128.
(28) Braeuer, J.; Gessner, T. A Hermetic and Room-Temperature Wafer Bonding Technique Based on Integrated Reactive Multilayer Systems. *J. Micromech. Microeng.* **2014**, *24* (11), 115002.
(29) Becker, C. R.; Apperson, S.; Morris, C. J.; Gangopadhyay, S.; Currano, L. J.; Churaman, W. A.; Stoldt, C. R. Galvanic Porous Silicon Composites for High-Velocity Nanoenergetics. *Nano Lett.* **2011**, *11* (2), 803−807.
(30) Parimi, V. S.; Lozda, A. B.; Tadigadapa, S. A.; Yetter, R. A. Reactive Wave Propagation in Energetic Porous Silicon Composites. *Combust. Flame* **2014**, *161* (11), 2991−2999.
(31) Parimi, V. S.; Tadigadapa, S. A.; Yetter, R. A. Control of Nanoenergetics Through Organized Microstructures. *J. Micromech. Microeng.* **2012**, *22* (5), 055011.
(32) Parimi, V. S.; Tadigadapa, S. A.; Yetter, R. A. Effect of Substrate Doping on Microstructure and Reactivity of Porous Silicon. *Chem. Phys. Lett.* **2014**, *609*, 129−133.
(33) Piekiel, N.; Churaman, W.; Morris, C.; Currano, L. Combustion and Material Characterization of Porous Silicon Nanoenergetics*IEEE 26th International Conference on Microelectromechanical Systems (MEMS), 2013*, Taipei, Taiwan, Jan 20−24, 2013; pp 449−452.
(34) Piekiel, N.; Churaman, W.; Morris, C.; Lunking, D. *Characterization of Patterened Galvanic Porous Silicon for On-Chip Combustion*. In *AIAA SciTech Conference Proceedings, 52nd Aerospace Sciences Meeting*, American Institute of Aeronautics and Astronautics: National Harbor, MD, 2014.
(35) Piekiel, N. W.; Morris, C. J.; Churaman, W. A.; Cunningham, M. E.; Lunking, D. M.; Currano, L. J. Combustion and Material Characterization of Highly Tunable On-Chip Energetic Porous Silicon. *Propellants, Explos., Pyrotech.* **2015**, *40*, 16−26.
(36) Piekiel, N. W.; Morris, C. J.; Currano, L. J.; Lunking, D. M.; Isaacson, B.; Churaman, W. A. Enhancement of On-Chip Combustion via Nanoporous Silicon Microchannels. *Combust. Flame* **2014**, *161* (5), 1417−1424.
(37) Plessis, M. d. A Decade of Porous Silicon as Nano-Explosive Material. *Propellants, Explos., Pyrotech.* **2014**, *39*, 348−364.
(38) Plummer, A.; Kuznetsov, V.; Joyner, T.; Shapter, J.; Voelcker, N. H. The Burning Rate of Energetic Films of Nanostructured Porous Silicon. *Small* **2011**, *7* (23), 3392−3398.
(39) Churaman, W.; Currano, L.; Becker, C. Initiation and Reaction Tuning of Nanoporous Energetic Silicon. *J. Phys. Chem. Solids* **2010**, *71* (2), 69−74.
(40) Churaman, W.; Currano, L.; Singh, A. K.; Rai, U. S.; Dubey, M.; Amirtharaj, P.; Ray, P. C. Understanding the High Energetic Behavior of Nano-Energetic Porous Silicon. *Chem. Phys. Lett.* **2008**, *464*, 198−201.
(41) Churaman, W. A.; Becker, C. R.; Metcalfe, G. D.; Hanrahan, B. M.; Currano, L. J.; Stoldt, C. R. Optical Initiation of Nanoporous Energetic Silicon for Safing and Arming Technologies. *Proceedings of SPIE* **2010**, 779506−779506−9.

DOI: 10.1021/acsami.5b01964
ACS Appl. Mater. Interfaces 2015, 7, 9889−9897

(42) Wang, S.; Shen, R.; Ye, Y.; Hu, Y. An Investigation into the Fabrication and Combustion Performance of Porous Silicon Nano-energetic Array Chips. *Nanotechnology* **2012**, *23* (43), 435701.
(43) Ashruf, C.; French, P.; Bressers, P.; Kelly, J. Galvanic Porous Silicon Formation Without External Contacts. *Sens. Actuators, A* **1999**, *74* (1 - 3), 118−122.
(44) Splinter, A.; Sturmann, J.; Benecke, W. New Porous Silicon Formation Technology Using Internal Current Generation with Galvanic Elements. *Sens. Actuators, A* **2001**, *92* (1 - 3), 394−399.
(45) Currano, L.; Churaman, W. Energetic Nanoporous Silicon Devices. *J. Microelectromech. Syst.* **2009**, *18* (4), 799−807.
(46) Savitzky, A.; Golay, M. J. E. Smoothing and Differentiation of Data by Simplified Least Squares Procedures. *Anal. Chem.* **1964**, *36* (8), 1627−1639.
(47) Incroprera, F. P.; DeWitt, D. P. *Introduction to Heat Transfer*, 3rd ed. John Wiley & Sons, Inc.: New York, 1996.
(48) Becker, C. R.; Currano, L. J.; Churaman, W. A.; Stoldt, C. R. Thermal Analysis of the Exothermic Reaction between Galvanic Porous Silicon and Sodium Perchlorate. *ACS Appl. Mater. Interfaces* **2010**, *2* (11), 2998−3003.

DOI: 10.1021/acsami.5b01964
ACS Appl. Mater. Interfaces 2015, 7, 9889−9897